J. Fluid Mech. (1995), *vol.* 301, *pp.* 51–64

Numerical investigation of Richtmyer–Meshkov instability using front tracking

By RICHARD L. HOLMES[1]†, JOHN W. GROVE[1] AND DAVID H. SHARP[2]

[1]Department of Applied Mathematics and Statistics, University at Stony Brook, Stony Brook, NY 11794-3600, USA

[2]Complex Systems Group, Theoretical Division, Los Alamos National Laboratory, Los Alamos, NM 87545, USA

(Received 10 June 1994 and in revised form 18 May 1995)

Front tracking simulations of the Richtmyer–Meshkov instability produce significantly better agreement with experimentally measured growth rates than obtained in non-tracking computations. Careful analysis of the early stages of the shock acceleration process show that nonlinearity and compressibility play a critical role in the behaviour of the shocked interface and are responsible for the deviations from the linear theories. The late-time behaviour of the interface growth rate is compared to a nonlinear potential flow model of Hecht *et al.*

1. Introduction

The quantitative understanding of the Richtmyer–Meshkov (shock-accelerated) interface instability has challenged scientists for over 30 years.

Interest in this instability is motivated by its importance in subjects such as inertial confinement fusion and supernovae dynamics.

The growth of perturbations at a shocked interface between two fluids was first studied in Richtmyer's seminal 1960 paper. In this paper he studied the solution of the linearized (compressible) Euler equations and found that after an initial rapid increase the growth rate in the linearized solutions oscillated about a limiting value. He also proposed an analytic formula for the growth rate based on an approximation to the full linear theory. The predictions of the analytic formula, known as the impulsive model, agreed quite well with the limiting value of the linear theory. In the time since Richtmyer's work this problem has been the subject of extensive investigation. The earliest experimental studies of this instability were performed by Meshkov (1970) who measured growth rates that were significantly smaller than the predictions of the impulsive model. More recent experiments by Benjamin (Benjamin 1992; Benjamin, Besnard & Haas 1993) also showed growth rates that were nearly half the value predicted by Richtmyer's theory. The lack of agreement between experiment and theory would ordinarily invalidate the theory. However, perturbation growth rates obtained by numerical simulation of experiments have agreed quite well with the linear theory (Benjamin *et al.* 1993; Cloutman & Wehner 1992; Meyer & Blewett 1972). Other simulations of the Richtmyer–Meshkov instability have also given

† Present address: Courant Institute of Mathematical Sciences, New York University, 251 Mercer Street, New York, NY 10012, USA.

growth rates very close to the values predicted by the impulsive model in the cases studied (several examples can be found in the volumes Besnard *et al.* 1991; Dannevik, Buckingham & Leith 1992; Linden, Youngs & Dalziel 1993), although interesting exceptions have been found by Mikaelian (1993) and Yang, Zhang & Sharp (1994).

In this paper we report progress consisting of substantially improved agreement between experiment, theory and computation. Our main tool is the use of the front tracking method to carry out highly resolved numerical simulations of certain experiments of Meshkov (1970) and Benjamin (Benjamin *et al.* 1993). Comparisons are made to measurements of the amplitude and amplitude growth rates of perturbations on the shocked interface. The computed growth rates are in excellent agreement with those found in Benjamin's experiments. In the case of Meshkov's experiments we obtain growth rates 60% higher than the experimentally measured values, but this still represents a substantial improvement over the results of previous simulations of these experiments.

The results of the simulations raise a number of important theoretical issues aside from the matter of agreement with experiment. The first concerns the relationship between the nonlinear theory and the small-amplitude theory, derived by linearizing the equations of motion. These theories agree for small initial amplitude perturbations and sufficiently early times, as expected. For larger amplitudes or later times there is an abrupt departure of the nonlinear theory from the linear theory. In §3 we explain this behaviour in terms of a re-acceleration of the interface by shocks produced by the (nonlinear) self-interaction of the reflected and transmitted waves. Another important issue concerns the long-time behaviour of the amplitude growth rate. In the simulations the growth rate is found to decay with time. Such behaviour has been predicted by Hecht, Alon & Shvarts (1994) on the basis of a nonlinear potential flow model for the fluid. Our numerical simulations are in general agreement with the results of this model, although they predict a slightly different decay rate. This cross-validation is important because the decay of the growth rate is not evident in the experiments of Meshkov or Benjamin, although it has been observed in other experiments (Aleshin *et al.* 1998; Meshkov 1992) and simulations (Meyer & Blewett 1972; Benjamin *et al.* 1993).

A third issue concerns the effect of varying numerical parameters. A discussion is given on the effect of variations in grid size, artificial viscosity and numerical surface tension on the computed growth rate of the instability.

2. Experimental configurations

We begin by specifying the experimental configurations which we model. Benjamin and Meshkov conducted their experiments in rectangular shock tubes in which two gases were initially separated by a thin membrane with an imposed single-wavelength sinusoidal perturbation. The membrane was ruptured by a plane shock propagating down the shock tube. Figure 1 shows a schematic representation of the geometry.

Benjamin's experiments used a Mach 1.2 shock in air incident on an interface with sulphur hexafluoride (SF_6). The interface perturbation had an amplitude of 0.24 cm and a wavelength of 3.75 cm. As these experiments were performed at the high-altitude Los Alamos National Laboratory we used ambient pressures of 0.8 bar and densities of 0.95 $g\,l^{-1}$ for air and 4.85 $g\,l^{-1}$ for SF_6 in our calculations. This corresponds to an initial Atwood ratio of 0.67. We used perfect gas equations of state with $\gamma_{air} = 1.4$ and $\gamma_{SF_6} = 1.09$.

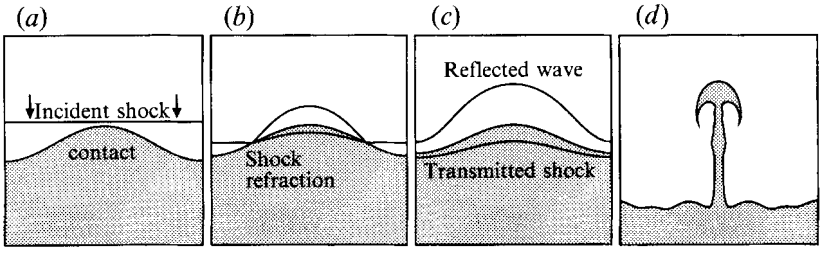

FIGURE 1. A schematic representation of the geometry in Richtmyer–Meshkov instability experiments. A shock wave collides with a material interface and is refracted. The reflected wave may be either a shock or a rarefaction depending on the fluid parameters and the shock strength. The instability consists of the growth in time of pertubations at the material interface. The last frame shows a possible late time configutration with a spike of heavy gas being injected into the lighter gas.

Meshkov's experiments were performed with a Mach 1.52 shock in air striking an interface separating the air from helium. The perturbation had an amplitude of 0.2 cm and a wavelength of 4 cm. A pressure of 1.013 bar and densities of 1.2 $g\,l^{-1}$ and 0.167 $g\,l^{-1}$ for air and helium, respectively, were used giving an initial Atwood ratio of 0.76. We assumed perfect gases with $\gamma_{He} = 1.63$.

The two experiments differed in the type of reflected wave produced. The shock refraction in Benjamin's experiment produced a reflected shock, while in Meshkov's experiment the refraction produced a reflected rarefaction. In both cases the rear wall of the tube was located sufficiently far from the interface that measurements of the growth rate could be made before the arrival of the shock reflected off this rear wall.

The quantities of interest in this study are the amplitude of the perturbations on the interface, $a(t)$, defined to be one-half the total interpenetration width, and the amplitude growth rate, $\dot{a}(t)$. These are the quantities which were measured in the experiments. Additional diagnostics produced from the computations, used in the analysis of the perturbations, include plots of the pressure and density fields of the flows and of the interface positions as a function of time. We also measured separately the flow velocities at the tips of the heavy gas spike and the light gas bubble. Note that $\dot{a}(t) = (v_{spike} - v_{bubble})/2$, where v denotes the velocity at the interface.

The main computational tool is the method of front tracking, which provides enhanced resolution and zero numerical diffusion in simulations of the shock acceleration process (Grove 1994; Chern *et al.* 1986). The main analytic methods are the small-amplitude theory (Richtmyer 1960; Yang *et al.* 1994) and comparison to a potential flow model recently derived by Hecht *et al.* (1994).

3. Comparison of the linear and nonlinear theories

If the initial interface perturbation is sufficiently small relative to the wavelength, linearized theories of the perturbation growth can be derived. A simple theory, due to Richtmyer (1960), is commonly used to estimate the growth rate of interface perturbations. Richtmyer begins with the linearized equations for Rayleigh–Taylor instability growth rates between incompressible fluids except that the constant gravitational acceleration is replaced by an impulsive one. If the perturbation is sinusoidal with wavenumber k the perturbation amplitude growth rate in the Richtmyer–Meshkov case is estimated as

$$\dot{a}(t) = kA\Delta u a(0+) \tag{3.1}$$

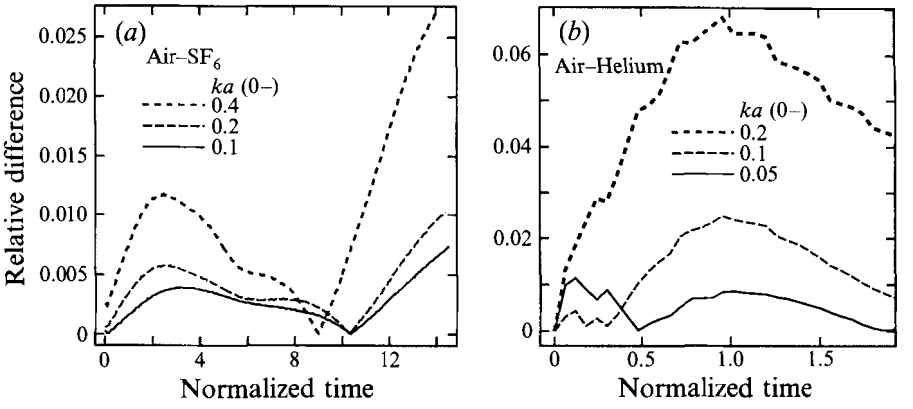

FIGURE 2. Convergence of the nonlinear simulations to the linearized solution for small amplitudes. A series of calculations was carried out for a set of three initial amplitudes of decreasing size, and (*a*) shocked air–SF_6 and (*b*) air–He interfaces. Amplitude convergence is measured in terms of the relative difference between the nonlinear and linear solutions, $|(a(t)-a_{lin}(t)|/|a_{lin}(t)|+|a(0-)|$ where $a(0-)$ is the initial amplitude of the pertubation. The horizontal axis is in dimensionless time units kc_0M_0t, where k is the wavenumber of the pertubation, c_0 is the sound speed in the air ahead of the incident shock and M_0 is the incident shock Mach number. One dimensionless time unit is equivalent to approximately 14 μs for air–SF_6 and 12.2 μs for air–helium.

as long as $ka(t) \ll 1$, where $A = (\rho_2^* - \rho_1^*)/(\rho_2^* + \rho_1^*)$ is the Atwood ratio using post-shock densities ρ_i^*, Δu is the change in translational velocity of the interface due to the action of the shock and $a(0+)$ is the shock-compressed amplitude. This is Richtmyer's impulsive model. Note that by starting with the equations for incompressible flow one is assuming that compressibility effects are negligible after the passage of the shock wave. Following Meyer & Blewett (1972) we use the average of the pre- and post-shock amplitudes rather than the post-shock amplitude in the case of a reflected rarefaction.

For $ka \ll 1$ one can linearize the Euler equations about the solution of the unperturbed problem (Riemann problem) and derive a set of PDE's in one space and one time dimension, along with boundary conditions. This approach is also originally due to Richtmyer, who considered the case of a reflected shock (Richtmyer 1960). More recently this method was extended to the case of a reflected rarefaction (Yang *et al.* 1994). Note that this linearization makes no incompressibility assumption.

We investigated the convergence of the nonlinear front tracking simulations to the linearized system by computing solutions for small initial amplitudes. Figure 2 shows the results of these computations for both the air–SF_6 and air–He cases. We measure convergence in terms of the relative amplitude difference

$$\frac{|a_{nonlin}(t) - a_{lin}(t)|}{|a_{lin}(t)| + |a(0-)|} \tag{3.2}$$

where $a_{linear}(t)$ denotes the amplitude as determined by the linear theory of Richtmyer and Yang *et al.* In both cases we obtain good convergence at early times, providing an important validation of our calculations.

In an attempt to explain the discrepancy between theory and Meshkov's experiments Sturtevant (1988) proposed a definition of the post-shock amplitude $a(0+)$ (in the case of a reflected shock) which was different from that used by Richtmyer and Yang *et al.* The nonlinear simulations of small-amplitude, early-time Richtmyer–Meshkov

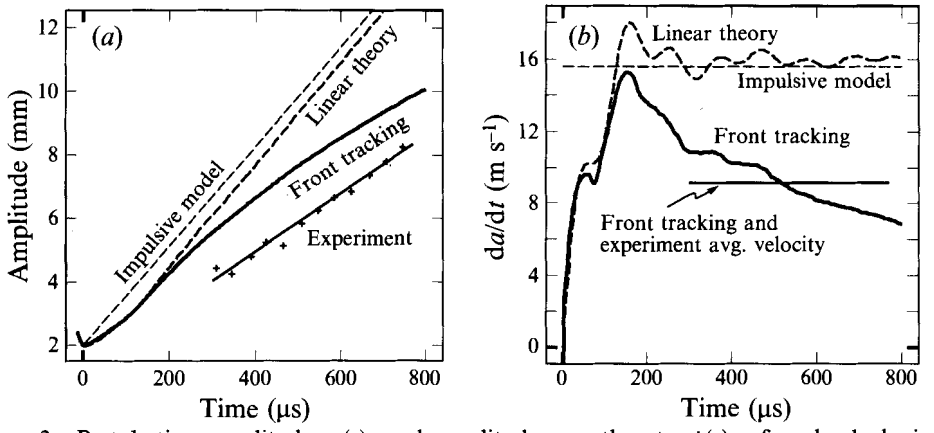

FIGURE 3. Pertubation amplitude, $a(t)$, and amplitude growth rate, $\dot{a}(t)$, of a shocked air–SF_6 interface measured in a frame moving with the interface. This graph compares the results of experimental averages, front tracking simulation, linear theory and Richtmyer's impulsive model. Also shown are results of a least-squares fit to the front tracking amplitude data over the period of experimental observation. Note that the front tracking average growth rate is indistinguishable from the experimental value in (*b*). The plus marks (+) show the results of one particular experiment.

instability presented here confirm that Richtmyer's definition is indeed correct and do not support the definition proposed by Sturtevant.

Figure 3 shows the amplitude and amplitude growth rates as given by the impulsive model, numerical solution of the linear theory, nonlinear simulations and experiment for the air–SF_6 case. We focus on two regions of the growth rate curves where divergence between the linear and nonlinear theories occurs. The first region of divergence begins at $t \approx 70\,\mu s$ with a reversal in the growth rate $\dot{a}(t)$ followed by a second period of rapid increase. The second region of divergence between the two theories occurs shortly after the maximum of $\dot{a}(t)$ is reached, at $t \approx 200\,\mu s$. Here the solution to the linearized equations saturates near this maximum value. In contrast, the nonlinear solution experiences a marked deceleration at this point.

The rapid deceleration of the shocked interface at time $200\,\mu s$ is an inherently nonlinear and compressible phenomenon. It can be understood in terms of a series of re-accelerations of the material interface by secondary shocks whose ultimate origins are self-interactions at the reflected and transmitted wave edges. As seen in the colour representations of the pressure field in figure 4, curvature in the reflected and transmitted waves generates additional shocks via nonlinear self-interaction. At $33\,\mu s$ these waves are clearly seen near the edges of the reflected shock (figure 4*a*). As the interaction proceeds the compression fronts steepen into shocks. These shocks collide near the tip of the spike at about $68\,\mu s$ as seen in figure 4(*b*), producing a high-pressure pulse near the interface that causes the growth rate to decrease. This deceleration corresponds to the first blip in the growth rate graph figure 3(*b*). At later times the waves emanating from the reflected and transmitted edges produce a series of criss-cross shock reflections. At approximately $207\,\mu s$ (figure 4*c*) a strong pulse crosses the interface, leading to the severe (and permanent) deceleration of the bubble. That this decrease is due primarily to action at the bubble side of the interface is clear from figure 5(*a*). By time $t = 344\,\mu s$ we see that the strong wave action has moved away from the interface region and the growth rate curve has smoothed considerably. Note the pair of Mach triple points at the far right of this figure.

Figure 6(*a*) shows pressure plots of the solution to the linearized equations and of the solution to the nonlinear Euler equations at time $t = 195\,\mu s$, near the time of the

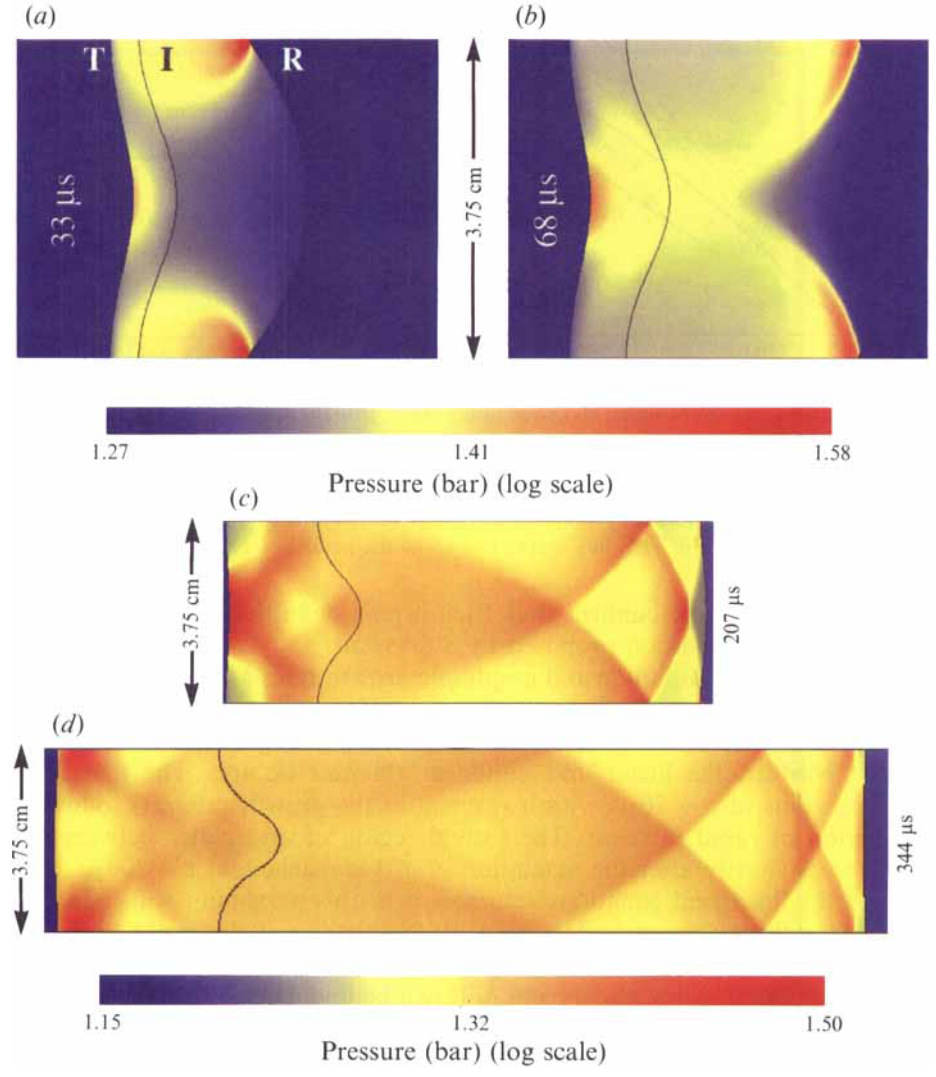

FIGURE 4. Pressure plots at a series of times for the nonlinear air–SF_6 solution. A cascade of shock waves generated by the self-interaction of the transmitted and reflected waves propagates back toward the interface and affects the perturbation growth rate at early and intermediate times. For reference we have labelled in the first frame the transmitted shock (T), the interface (I) and the reflected shock (R). Note that the colour map has been adjusted so that the full range of colour occurs within the region of interest (between the transmitted and reflected shocks). The blue regions at the left and right have pressures of 0.8 bar and 1.1 bar, respectively.

most extreme divergence of the two solutions. We call attention to two important features of linear solutions: they do not allow the focusing of characteristics and the linearization constrains the geometry of the wave fronts to be sinusoidal. These two restrictions prevent the production of the additional shocks that are present in the nonlinear solution, i.e. there is no cascade of reflected shocks from the self-interaction of the transmitted and reflected waves. The linear solution displays a series of acoustic waves, but they do not sharpen into shocks and are thus much weaker than the corresponding waves of the nonlinear solution. We should note that the strong

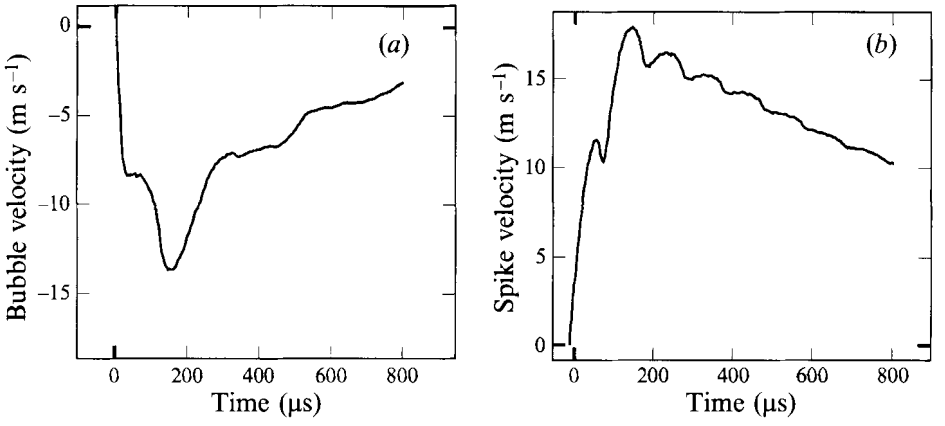

FIGURE 5. (*a*) Bubble and (*b*) spike velocities at a shocked air–SF_6 interface. the full amplitude growth rate shown in figure 3 is $\dot{a}(t) = (v_{spike} - v_{bubble})/2$. Note how certain events in the amplitude growth rate occur at either the spike of the bubble, but not both.

waves in the nonlinear solution come in pairs and thus we have two pressure maxima as we cross the tube in the x-direction. This is in contrast to the linear theory in which all quantities are assumed to have sinusoidal perturbations and, hence, a single maximum and minimum value.

The analysis of secondary waves can be followed further in time to account for the plateau in $\dot{a}(t)$ during the observation period. We note that during the observational window this ringing of waves near the interface subsides. It is at this point that the hypotheses of the potential flow model begin to be satisfied, as discussed in the next section.

Figure 6(*b*) shows a similar comparison between the nonlinear and linear theories for the air–helium case. The figure shows the pressure field at 65 μs, near the time of rapid divergence between the growth rate predictions of nonlinear and linear theories. As with the air–SF_6 case there is a significant amount of nonlinear behaviour that is not captured by the linearized theory. Specifically, the waves generated by the transmitted shock self-interaction have sharpened considerably and steepened into shocks by this time. We observe that high-pressure regions have formed above the bubble tips along the edges of the nonlinear simulation plot creating a pressure gradient opposing the bubble motion. This gradient is not evident in the linear solution.

4. Late-time asymptotics

Hecht *et al.* (1994) have developed a model for bubble growth in the Richtmyer–Meshkov instability that is based on three hypotheses: (*a*) incompressibility after the passage of the shock over the interface, (*b*) irrotational flow in the region of the bubble tip, so that the physics can be described by a potential flow, and (*c*) the Atwood ratio is near 1. Their model predicts an asymptotic single bubble velocity given by

$$v_{bubble} = \frac{1}{3kt/2} \tag{4.1}$$

where k is the wavenumber of the perturbation and t is the time. Note that this velocity is measured in a frame moving with the velocity of an unperturbed interface.

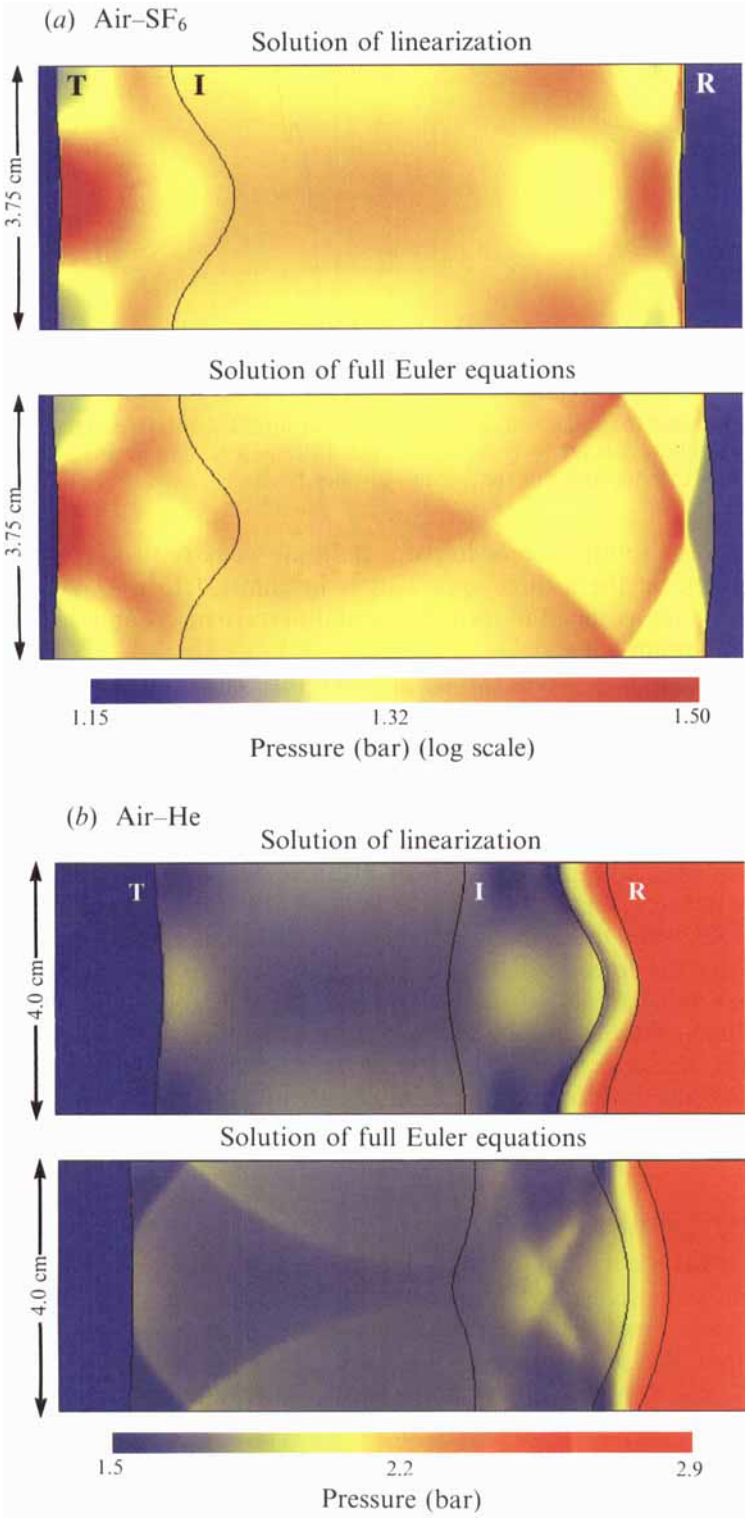

FIGURE 6. For caption see facing page.

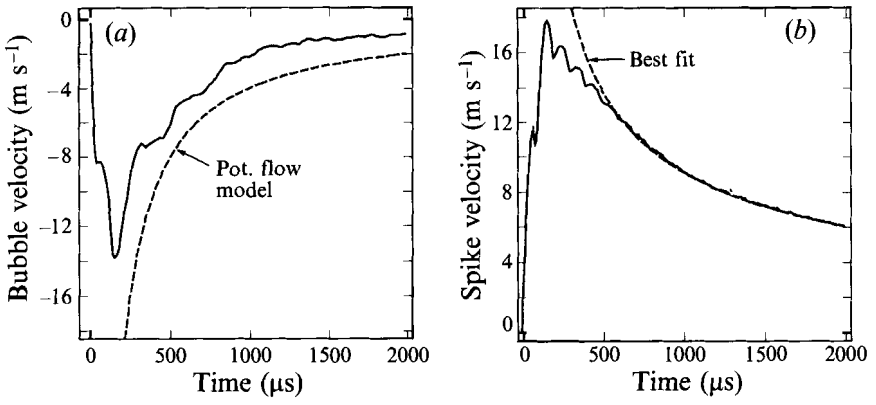

FIGURE 7. Computation of the bubble and spike velocities at late times for the case of an air–SF_6 interface. For the bubble velocity we show a comparison with the asymptotic value predicted by the potential flow model, $2/(3kt)$. For the spike velocity we show a comparison to a fit from 500 μs.

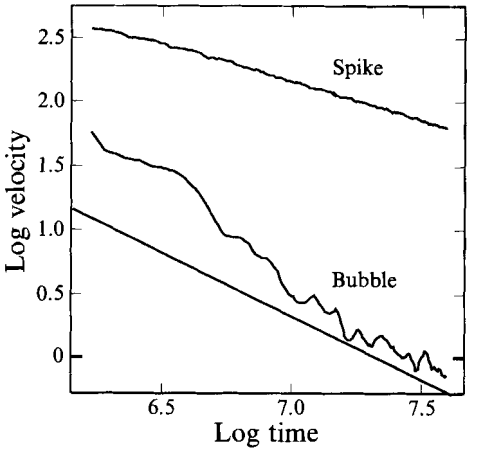

FIGURE 8. Log time *vs.* log velocity for bubble and spike velocities. The spike velocity is fit by a line while the bubble velocity is shown with a reference line with slope −1 for comparison with the decay rate predicitons of the potential flow model.

Figure 7(*a*) shows v_{bubble} from the nonlinear simulations compared to equation (4.1). Figure 8 shows that the decay rate of the numerical simulation is of the same magnitude as that predicted from the theory, although it appears slightly lower. We note that the post-shock Atwood ratio is only 0.70. We also observe an offset between the potential flow and simulation velocity curves. Note that this model applies only to bubbles and not to spikes. We also emphasize that the effects of compressibility remain important at times significantly later than the time of passage of the initial shock through the interface. Indeed, the velocity offset is likely to be due in part to

FIGURE 6. A comparison of the linear and nonlinear solutions. (*a*) air–SF_6 at $t = 195$μs. We see that the linear solution does not show the strong wave action that affects early and intermediate time growth rates in the nonlinear solution. (*b*) air–helium at $t = 65$μs. Again there is significant nonlinear wave activity which is not captured by the linearized solution. In both frames we have again labelled the transmitted and reflected waves as well as the interface. In the air–helium case we have labelled the leading and trailing edges of the reflected rarefaction by (R).

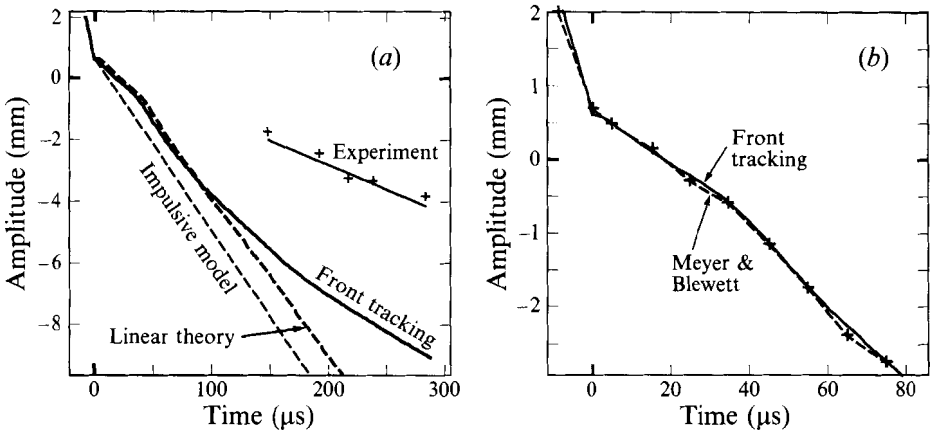

FIGURE 9. (*a*) Pertubation amplitude, $a(t)$ of a shocked air–helium interface. The figure compares the results of simulation, linear theory, impulsive model, and experiment. (*b*) Enlargement showing early-time agreement between the front tracking results and those of Meyer and Blewett (+).

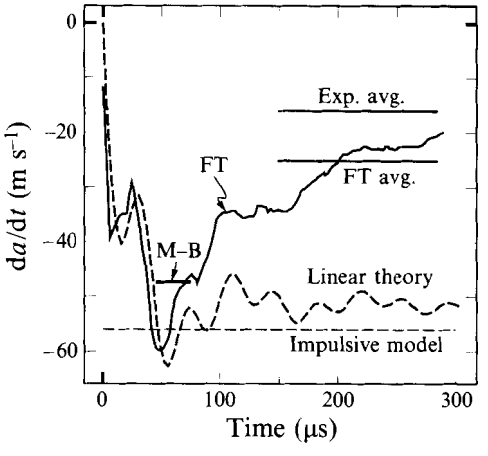

FIGURE 10. Pertubation amplitude growth rate, $\dot{a}(t)$, of a shocked air–helium interface. The figure compares the results of simulations (including those of Meyer & Blewett), linear theory, impulsive model and experiment.

the fact that the early-time compressible wave interactions discussed in the previous section are not properly included in the incompressible potential flow model.

It is interesting to note that the spike velocity can be fit by a power law. Figure 7(*b*) is a plot of v_{spike} and a fit of the data given by $v_{spike} = 510t^{-0.58}$. As seen in figure 8 the fit to the data is excellent from time $t = 500\,\mu s$ to the end of the simulation. This decay in bubble and spike velocities should be contrasted with the single-mode Rayleigh-Taylor instability, in which the bubble approaches a constant velocity while the spike undergoes constant acceleration for an Atwood ratio $A = 1$ and approaches a constant velocity for $A < 1$.

5. Comparison to experiments

Figures 9 and 10 show a comparison of simulations with experiment for the air–He case. The numerical simulations give growth rates 60% higher than those reported by Meshkov (1970). We reiterate that the full scale simulations of the air–He experiment do agree with the linear theory at small times.

We compared our computed growth rates to simulations by Meyer & Blewett (1972). These authors reported growth rates 200% higher than thoses measured by Meshkov. However, Meyer & Blewett reported growth rates for times earlier than the times of observation in Meshkov's experiments. Referring to figures 9(*b*) and 10, we see that the time interval for which Meyer & Blewett reported growth rates corresponds to the peak in $\dot{a}(t)$. We observe that by the times for which Meshkov measured the growth rate there had been significant decay in this quantity. This may account for some part of their overshoot.

Comparison of simulations to experiments in the air–SF_6 case results in excellent agreement for the growth rates (see figure 3 and Grove *et al.* 1993). However, there is a significant offset in the value of the absolute amplitude of the perturbations. The offset between the computational and experimental values for the perturbation amplitude is even more severe in the air–He case. This may be due to mass diffusion in the experiments, which is more significant with an air–He interface than with air–SF_6.

The improved agreement between the front tracking simulations and experiment is due to the sharp resolution of the interface. Tests using untracked shock waves have shown that the growth rates are very similar to those found in the fully tracked simulations except at early times. This is consistent with the analysis given in §3 of the wave action generated by shock self-interaction. Differences in the transmitted and reflected shocks will be felt most strongly when the waves are closest to the interface and thus the effects of an untracked shock will be most significant at early times.

We know of no model that provides quantitative estimates of the effect of the membrane in Meshkov's and Benjamin's experiments. We have shown that it is not necessary to invoke membrane effects to achieve agreement with Benjamin's measured growth rate. This does not mean membrane effects have been ruled out. They could well have an effect on the early-time behaviour (not covered in Benjamin's data) and possibly account for the residual discrepancy in the amplitude. The situation is of course more open in the Meshkov experiment. The best way to resolve the issue of membrane effects is to perform Richtmyer–Meshkov instability experiments in which membranes are not used.

A detailed discussion of membrane effects is beyond the scope of this paper. We note, however, that the computational approach to estimating membrane effects is not promising. Analysing the deformation and fragmentation of a thin elasto-plastic membrane would add severe demands to an already demanding computation. There is no established and benchmarked methodology for modelling the fragmentation of such a membrane. Even if one did come up with a model of membrane dynamics, it would be very difficult to know that it is correct. Since such a model is likely to require phenomenological parameters: simply fitting these parameters to obtain agreement with experiment would accomplish very little.

6. Numerical validation

We conducted several tests to validate our numerical methods. Convergence to the linear theory at small times was discussed above.

We also investigate convergence under mesh refinement. The air–He amplitude growth rates have converged at a resolution of 100 zones per wavelength (figure 11). The results for the air–SF_6 case are somewhat more complicated. The bubble velocity converges at a resolution of 125 zones per wavelength, as shown in figure 12, while the spike velocity continues to increase as the mesh is refined. Several factors may

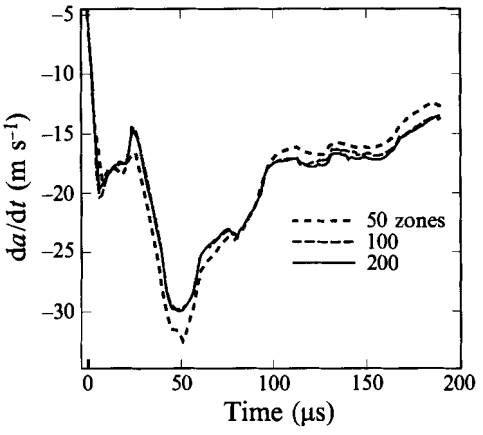

FIGURE 11. Mesh refinement tests for the air–He simulations.
We see convergence in the growth rate by 100 zones per wavelength.

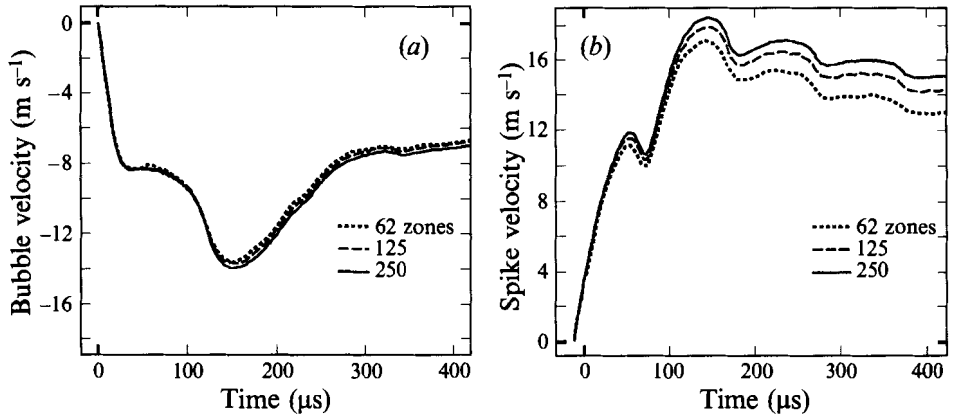

FIGURE 12. Mesh refinement tests for the case of an air–SF_6 interface. Results for computations at resolutions of 62, 125, and 250 zones per wavelength are shown (*a*) Bubble velocity; (*b*) spike velocity. The bubble velocity has converged but the spike velocity increases with increasing resolution.

contribute to this behaviour. First, there is considerably more wave activity near the tip of the spike than at the tip of the bubble which may require more resolution to achieve convergence. In addition, the theoretical convergence of the numerical solution naturally occurs in the L^1 norm rather than the L^∞ norm being measured here. The results shown in figure 3 for air–SF_6 are found using a grid of 125 zones per wavelength since we do not have the computational resources to run the 250 zone simulation to late times. However, it is clear from the results of the shorter simulations in figure 12(*b*) that the difference between spike velocities at 250 zones and 125 zones is approximately half the difference between 125 zones and 62 zones, which is consistent with first-order convergence near the fronts. To estimate the error in the 125 zone simulation we note that for a first-order scheme the reduction in error achieved by refining the grid from $\Delta x = h$ to $\Delta x = h/2$ is the same as the reduction from $\Delta x = h/2$ to the value under full mesh refinement, i.e. $\Delta x \to 0$. Since the change in spike velocity from 62 zones to 125 is approximately 10% we estimate that there is an error of 10% in the spike velocity calculated at 125 zones. Because the changes in the full amplitude growth rate $-(v_{spike} - v_{bubble})/2-$ are one-half the changes in the

spike velocity, and given that the bubble velocity has converged, we conclude that the error in the growth rate at 125 zones is approximately 5%.

We also studied the influence of artificial viscosity and numerical surface tension on the amplitude growth rate. It is found that the growth rates are insensitive to these parameters.

7. Conclusion

The analysis of the simulations shows that compressibility and nonlinear wave interactions play an important role in the early-time development of the Richtmyer–Meshkov instability, up to and including the time measured in experiments. These wave interactions are not captured in the linearized theories commonly used to estimate perturbation growth rates. In addition the late-time behaviour of the interface, after compressibility effects have subsided, agrees qualitatively with the model of Hecht *et al.*

Front tracking and the proper timing of growth rate measurements lead to improved agreement between experiment and simulation perturbation growth rates. It appears worthwhile to study the effect of mass diffusion on the early-time growth of the perturbations to aid in understanding the still unresolved difference in amplitudes.

We give our thanks to James Glimm for his encouragement and guidance. This work has been supported by the U.S. Army Research Office the Mathematical Sciences Institute of Cornell University under subcontract to SUNY Stony Brook, ARO contract number DAAL03-91-C-0027, the National Science Foundation, Grant no. DMS-9057429, the National Science Foundation, Grant no. DMS-9201581, the U.S. Army Research Office, Grant no. DAAL03-92-G-0185 and the U.S. Department of Energy.

REFERENCES

ALESHIN, A. N., GAMALLI, E. G., ZAITSEV, S. G., LAZAREVA, E. V., LEBO, I. G. & ROZANOV, V. B. 1988 Nonlinear and transitional stages in the onset of the Richtmyer-Meshkov instability. *Sov. Tech. Phys. Lett.* **14**, 466–468.

BENJAMIN, R. 1992 Experimental observations of shock stability and shock induced turbulence. *Advances in Compressible Turbulent Mixing* (ed. W. Dannevik, A. Buckingham & C. Leith), pp. 341–348. National Technical Information Service, US Department of Commerce 5285 Port Royal Rd. Springfield VA 22161.

BENJAMIN, R., BESNARD, D. & HAAS, J. 1993 Shock and reshock of an unstable interface. *LANL Rep.* LA-UR 92-1185. Los Alamos National Laboratory.

BESNARD, D., CAVAILLER, C., DAGENS, L., FIGEAC, P., DE GLINIASTY, M., HAAS, J., HOLSTEIN, P., MONTIGNY, J., PARISOT, C., RUPERT, V., SITT, B. & WILKE, N. (Eds.) 1991 *Proc. Third Intl Workshop on the Physics of Compressible Turbulent Mixing at Royaumont, France.* CEA DAM.

CHERN, I.-L., GLIMM, J., MCBRYAN, O., PLOHR, B. & YANIV, S. 1986 Front tracking for gas dynamics. *J. Comput. Phys.* **62**, 83–110.

CLOUTMAN, L. D. & WEHNER, M. F. 1992 Numerical simulation of Richtmyer-Meshkov instabilities. *Phys. Fluids* A **4**, 1821–1830.

DANNEVIK, W., BUCKINGHAM, A. & LEITH, C. (Eds.) 1992 *Advances in Compressible Turbulent Mixing.* National Technical Information Service, US Department of Commerce 5285 Port Royal Rd. Springfield VA 22161.

GROVE, J., HOLMES, R., SHARP, D. H., YANG, Y. & ZHANG, Q. 1993 Quantitative theory of Richtmyer-Meshkov instability. *Phys. Rev. Lett.* **71**, 3473–3476.

GROVE, J. W. 1994 Applications of front tracking to the simulation of shock refractions and unstable mixing. *J. Appl. Numer. Math.* **14**, 213–237.

HECHT, J., ALON, U. & SHVARTS, D. 1994 Potential flow models of Rayleigh-Taylor and Richtmyer-Meshkov bubble fronts. *Phys. Fluids* **6**, 4019–4030.

LINDEN, P. F., YOUNGS, D. L. & DALZIEL, S. B. (Eds.) 1993 *Proc 4th Intl Workshop on the Physics of Compressible Turbulent Mixing*. Cambridge University Press.

MESHKOV, E. E. 1970 Instability of a shock wave accelerated interface between two gases. *NASA Tech. Trans.* **F-13**, 074.

MESHKOV, E. E. 1992 Instability of shock-accelerated interface between two media. In *Advances in Compressible Turbulent Mixing* (ed. W. Dannevik, A. Buckingham & C. Leith) 473–503. National Technical Information Service, US Department of Commerce 5285 Port Royal Rd. Springfield, VA 22161.

MEYER, K. A. & BLEWETT, P. J. 1972 Numerical investigation of the stability of a shock-accelerated interface between two fluids. *Phys. Fluids* **15**, 753–759.

MIKAELIAN, K. O. 1993 Growth rate of the Richtmyer-Meshkov instability at shocked interfaces. *Phys. Rev. Lett.* **71**, 2903–2906.

RICHTMYER, R. D. 1960 Taylor instability in shock acceleration of compressible fluids. *Commun. Pure Appl. Maths.* **13**, 297–319.

STURTEVANT, B. 1988 Rayleigh-Taylor instability in compressible fluids. In *Proc 16th Intl Symp on Shock Tubes and Shock Waves, Aachen W. Germany July 26-32, 1987* (ed. H. Gronig). VCH.

YANG, Y., ZHANG, Q. & SHARP, D. H. 1994 Small amplitude theory of Richtmyer-Meshkov instability. *Phys. Fluids* **6**, 1856–1873.